Nanometer-scale surface modification of Ti6Al4V alloy for orthopedic applications

Xie, Jianhui; Luan, Ben Li

Publisher's version / Version de l'éditeur:
https://doi.org/10.1002/jbm.a.31359
Journal of Biomedical Materials Research Part A, 84A, 1, pp. 63-72, 2007-06-28

Nanometer–Scale Surface Modification of Ti6Al4V Alloy for Orthopedic Applications

Jianhui Xie and Ben Li Luan*

Integrated Manufacturing Technologies Institute

National Research Council

800 Collip Circle, London, Ontario Canada N6G 4X8

** Corresponding author, E-mail: ben.luan@nrc-cnrc.gc.ca,*

Ph: +1-519-430-7043, FAX: +1- 519-430-7064

Abstract

This communication presents a novel technology to enhance the biocompatibility of bioinert Ti6Al4V alloy as implant materials for orthopaedic application. The surface of Ti6Al4V alloy was electrochemically activated in NaOH solution to create a porous structure with nanometer topographic features and an alkaline environment, thus promoting the formation of bone-like hydroxyapatite coating and enhancing the bonding strength of the coating. This innovative activation process was proved to be effective and essential. The activated surface was confirmed to be pure TiO_2 and the formed coating was characterized of pure hydroxyapatite with a

nanometer-scaled grain size structure by means of XPS, FESEM/SEM/EDX, XRD and TEM techniques.

Key Words: Electrochemical activation, Titanium oxide, nanometer scale, Ti6Al4V alloy, hydroxyapatite coating

1. Introduction

Titanium (Ti) and titanium alloys are classified as bioinert materials due to a stable oxide layer formed on the surface [1-4]. They have been extensively investigated and applied as implant materials due to their combined properties of corrosion resistance, biocompatibility and mechanical performance [5]. However, these artificial materials implanted into bone defects are generally encapsulated by fibrous tissue thus they are isolated from the surrounding bone [5, 6], which hinders the growth of bone into the implants and results in weak bonding between the bone and the implants. This requires a surface modification to promote the ingrowth of human bone into the implanted biomaterials, thereby forming a natural and smooth connection between bone and biomaterials.

Surface properties such as wettability, chemical composition and topography govern the biocompatibility of titanium. Surface roughness on the nanometer-scale has been shown to favor promoting smooth connection between bone and the implants and reducing fibrous tissue encapsulation [5]. However, conventionally processed (e.g. cast, forged, etc) titanium currently

used for orthopedic and dental applications exhibits roughness only on a micrometer level but is smooth on a nanometer scale [7]. An approach was therefore attempted to design the next-generation of implants focusing on creating unique nanometer-topography (or roughness) on the implant surface, simulating the nano-structures such as collagen and hydroxyapatite in natural bone.

The calcium phosphate ceramics are classified as bioactive materials which create a direct chemical bonding between implant and surrounding bone [5]. Much attention has focused on ceramics which resemble the mineral phase in bone tissues, i.e. hydroxyapatite (HA), octacalcium phosphate and tricalcium phosphate [5, 8-11]. Probably the most interesting bioceramic development in recent years is the bioactive phosphate coatings onto prosthetic components using different coating techniques [12-23], e.g. plasma spray, biomimetic, electroplating, electrophoretic deposition, sol-gel, etc.

To take advantage of the excellent characteristics of Ti-alloys and avoid the fibrous tissue encapsulation around the Ti implants, the growth of apatite coating onto the Ti-alloy is extensively investigated [6, 11-14, 24, 25]. If the formed apatite is very similar to bone mineral in its composition and structure, osteoblasts preferentially proliferate and differentiate to produce apatite and collagen on this apatite layer, and consequently the surrounding bone can come into direct contact with the apatite layer. When this occurs, a strong chemical bond is formed between the bone and the apatite layer on the surface of implants, indicating that the essential requirement for a living bone to bond to an implant is the formation of a biologically active bone-like apatite layer at the interface.

Human body fluid is supersaturated with respect to apatite even under normal conditions [6]. The fact that apatite formation only occurs in bone tissue in the human body is attributed to the high activation energy for the homogeneous nucleation of apatite in the human body fluid. Therefore, if an artificial material has a favorable condition, apatite will easily nucleate on its surface. Once the apatite nuclei are formed, they would spontaneously grow by consuming calcium and phosphate ions from the surrounding body fluid [6].

Currently some of the researchers in the field of apatite coating on the titanium alloys are applying chemical methods to activate the surface [6, 8, 14, 18, 26-30]. During these chemical activation treatments, the titanium alloy is treated in NaOH solution of various concentrations at elevated temperatures, followed by heat-treatment. These procedures need several long steps and usually take 3 days to prepare the samples for the formation of apatite. Some other researchers [25, 27] are applying autoclave heating to treat the Ti-alloy at high temperature with high concentration of NaOH solution. These procedures also are time-consuming and require special equipments.

In our laboratory, an electrochemical method was discovered to effectively treat the surface of Ti-alloy. The treatment can be easily conducted at room temperature and requires only a short period of time (as short as 30 minutes). Using this novel method, a favorable surface condition was created which enabled successful subsequent formation of hydroxyapatite coating. In this investigation, the coating approach is termed "chemo-biomimetic HA coating process" for two reasons: 1) the deposition is based on the conventional biomimetic process simulating the natural

bone growth, and 2) chemical modifications were conducted to the substrate surface chemistry prior to HA deposition as well as to the composition of deposition solutions, more specifically, increased calcium and phosphate concentrations.

2. Experimental Details

2.1 Materials and Preparation of Samples

A Ti6Al4V alloy (RMI Titanium Company, Mississauga, Canada), a very popular biomaterial, was chosen as the testing material with a chemical composition (*wt* %) as follows: 0.12 O, 0.02 C, 0.008 N, 0.213 Fe, 6.16 Al, 3.92 V and balanced Ti. The specimens were sheared from a rolled plate (1.7mm thick) to the dimension of $10\times10mm^2$, mechanically polished using SiC paper #400 and #600, and 9μm Al_2O_3 paper. The polished samples were ultrasonically cleaned in acetone, ethanol and deionized water (Millipore Elix 10 system, resistance $\geq$ 15MΩ-cm) for 10 minutes, separately. The clean specimens were etched in a 0.2 vol. % HF (Caledon, 48%) + 0.4 vol. % HNO_3 (Fisher, 68-71%) solution for 10 minutes, rinsed thoroughly with deionized water, and subjected to ultrasonic cleaning for 10 minutes in deionized water and then dried at room temperature. The specimens were ready for the further electrochemical activation treatment.

2.2 Electrochemical Activation of Ti6Al4V Alloy

The electrochemical activation treatment on Ti6Al4V alloy was carried out at room temperature in a 5M NaOH solution. A potentiostatic polarization at 200mV (vs, $Hg/HgSO_4$) was applied for 5 hours using an EG&G M273A potentiostat with a platinum plate as the cathode. Afterwards the treated specimen was gently and thoroughly rinsed using deionized water and was ready for the apatite formation.

To make the electrochemical activation treatment simpler and less expensive, another electrochemical treatment was carried out using HP E3610A DC power supply, a potentiostatic voltage of 5V was applied between the Ti6Al4V specimen as the anode and a platinum cathode. This treatment was conducted for 30 minutes at room temperature in 5M NaOH solution.

An activation treatment using chemical method [5] was also conducted to compare with the electrochemical methods. The Ti6Al4V alloy samples were treated in 5M NaOH solution at 95°C for 5 hours, thoroughly rinsed with deionized water, dried and then subjected to heat treatment at 600°C for one hour. The heating and cooling ramping rate is 3°C/min.

2.3 Characterization of the Activated Ti6Al4V Alloy

X-ray photoelectron spectroscopy (XPS) is a very surface sensitive analytical technique and, as such, provides elemental and chemical state data from the outer 5-10 nm of a surface. Survey (pass-energy of 160eV) and high-resolution spectra (pass energy 20eV) for Ti 2p and O 1s peaks were obtained for each sample. XPS was carried out with a Kratos AXIS Ultra spectrometer using a monochromatic Al Kα source (20mA, 14kV). The instrument was calibrated to give a

binding energy (BE) of 83.96eV for the Au $4f_{7/2}$ line for metallic gold and the spectrometer dispersion was adjusted to give a BE of 932.62eV for the Cu $2p_{3/2}$ line of metallic copper. The Kratos charge neutralizer system was used on all specimens. Survey spectra were collected with a pass-energy of 160eV and an analysis area of ~300×700 μm^2. High-resolution spectra were obtained using a 20eV pass-energy and an analysis area of ~300×700 μm^2. All high-resolution spectra were charged reference to adventitious carbon at 285.0eV. Spectra were analyzed using CasaXPS software (version 2.2.19) (Fairley Inc, 1999-2003).

Nanometer-scale surface morphologies of the activated Ti6Al4V alloy were observed using Hitachi S-4500 field emission SEM (FESEM) equipped with an EDAXTM EDX system. At high electron beam voltages (>15kV) a spatial resolution of <2 nm is possible.

Measurement of surface pH range was conducted using different pH indicators on the activated substrate. One drop of the indicator solution was applied onto the prepared substrate surface. The pH range was detected based on the color change of the indicators.

2.4 Apatite Formation on the Activated Specimens

The apatite coating was formed in a solution with Ca^{2+} and HPO_4^{2-}concentrations enhanced by a factor of five, 5(Ca&P), shown in Table 1, as compared with the conventionally used simulated body fluid (SBF) and blood plasma [30]. The chemicals used for the coating solution are reagent grade, including NaCl (Fluka, ≥99.5%), $NaHCO_3$ (Sigma-Aldrich, ≥99.7%), KCl (Fisher, ≥99.6%), Na_2HPO_4 (Sigma-Aldrich, >99.0%), $MgCl_2.6H_2O$ (Sigma-Aldrich, >99.0%),

$CaCl_2.6H_2O$ (Fisher, ≥99.5%), Na_2SO_4 (Anachemia, >99.0%). The apatite formation in the 5(Ca&P) solution was conducted in beakers using the chemo-biomimetic method. The solution was buffered at pH of 6.50, and the beakers containing coating solution were immersed in a water bath at 37°C. Apatite deposition proceeds on the activated Ti6Al4V alloy at an average deposition rate of 5.0 μm/hr. The deposition rate is calculated based on the coating thickness, observed under SEM, and the duration of deposition. The solution was replenished with fresh solution at 30min intervals.

The observation of surface morphologies of the hydroxyapatite coating was conducted using Hitachi S-3500N SEM/EDX with a practical spatial resolution of 100nm. The nanometer grain size of formed hydroxyapatite coating was characterized using Philips CM20 Transmission Electron Microscope (TEM). The coating was scratched off of the Ti6Al4V alloy substrate, dispensed in Ethanol, attached on a copper screen mesh for TEM analysis. The coating was also scratched off of the coated substrates and to collect a sufficient amount of powder for XRD analysis. XRD analysis was carried out using a Bruker D8 diffractometer with Cukα radiation. The scan was conducted from 10 to 70° at a step size of 0.02°.

3. Results and Discussion

Bonding strength is an important factor in a successful implantation of artificial joints. Bare Ti6Al4V alloy creates capsulation of soft issues between the bone and the artificial joints, and it takes a long time for the bone to grow together with the artificial joints. The surface of the

Ti6Al4V alloy for artificial joint should therefore be bioactive with favorable topographic features for the anchoring and ingrowth of bone. In addition to the nanometer-scale roughness with bioactive TiO_2 on top, a layer of bioactive hydroxyapatite coating on such features will further enhance the bone ingrowth.

Fig. 1 shows the surface nano-structure of electrochemically activated Ti6Al4V alloy. The surfaces are covered by evenly distributed pores with size of less than 200nm for the constant-potential activated sample (Fig. 1a), and less than 100nm for the constant-voltage activated sample (Fig. 1c). At higher magnifications (Figs. 1b and 1d), the microstructure of the surface is a bone-like network of pores. The pores are larger for the constant-potential activation (Figs. 1a and 1b) than the constant-voltage activation (Figs. 1c and 1d). This is possibly due to the longer time of polarization. The surface of the constant-voltage polarized Ti6Al4V alloy shows the ridges and uneven surface formed during acid etching (Fig. 2) before the activation procedure. As for the constant-potential-activated Ti6Al4V samples with an extended period of 5 hours, the ridges of the etched substrate were dissolved away thereby leveling off the surface, and at the same time forming a nanometer-pore network structure. While the chemical acid etching process creates ridges and valleys of micrometer scale, the electrochemical activation further creates new nanometer pores on these similar microstructures. These nanometer features imbedded on the microstructures favor the anchoring and ingrowth of bone into the implants, potentially resulting in a stronger bonding at the interface.

In addition to the electrochemical treatment described above, a chemical treatment was also applied on the Ti6Al4V alloy to modify the surface for deposition and growth of hydroxyapatite

coating. Fig. 3a shows the surface nano-structure of chemically activated Ti6Al4V alloy. Similarly, the surface is also covered with bone-like network of pores, but the chemically treated specimen has much larger and less uniform pore size at less than 500nm, while with the long period of activation, the ridges of the acid-etched surface was completely dissolved and a more leveled surface, compared with electrochemically activated surface, was obtained with a nanometer-pore structure. The micro-roughness associated with the ridged surface is reduced or eliminated due to extensive dissolution. This leveling of the surface makes the anchoring of bone ingrowth potentially less effective. Higher magnification of the pores (Fig. 3b) illustrates that the pores are coalesced in certain area due to the excessive dissolution. Also, the chemical activation process is time consuming and the treated surface needs subsequent heat treatment. In summary, compared to chemical treatment, the electrochemical constant-voltage activation is a simpler process without heat treatment and with a much shorter duration. Further it also forms nanostructures beneficial to the bone ingrowth that are not attainable from chemical treatment.

Another purpose of the activation treatment is to create titanium oxide on the surface to further promote the formation of hydroxyapatite coating, which starts from the reaction between Ca^{2+} and TiO_2 (6, 17). The XPS analysis shows that the surface was completely converted to TiO_2 during activation (Fig. 4). The Ar^+ sputter cleaned Ti6Al4V specimen (Fig. 4a) showed two peaks at the binding energies of 460.0eV and 453.9eV, attributable to Ti 2p1/2 and Ti 2p3/2 peaks, respectively. The mechanically polished and acid etched specimens (Fig. 4b and 4c), which were air-exposed, showed the most dominant peak at ~459eV, a second dominant peak at ~465eV, and a small third peak at ~454eV. The first two dominant peaks were mostly attributed to oxidized titanium with a minor contribution of Ti metal 2p1/2 at 460.1eV. The small third

peak at 453.9eV was attributed to Ti metal 2p3/2. Comparing to the sputter cleaned surface, there is also evidence of the presence of sub oxides (e.g. TiO_{2-x}, TiO_{2-y}, and TiO). However, the Ti metal peaks were still shown in the spectrum since the oxide formed was very thin (less than 5-10 nm in thickness), but Ti metal 2p3/2 peak decreased significantly as oxide was formed on the specimen surface. High resolution XPS spectrum of Ti 2p peaks obtained for the chemically (Fig. 4d) and electrochemically (Fig. 4e) activated specimens showed no Ti 2p metal components, suggesting the formation of a thicker oxide layer on the surface (>5-10 nm). Both Ti 2p peaks corresponded to Ti^{4+} valence state, indicating that suboxides such as TiO, Ti_2O_3 or Ti_3O_5 were not present on the oxide surface.

The O 1s peaks (Fig. 5) were fitted with three different components, lattice oxide (O^{2-}), hydroxide (physisorbed -OH), and water (chemisorbed H_2O). All the specimens showed a major peak at 530.5 ± 0.3 eV, which is attributed to lattice oxide. Minor O 1s peaks at higher binding energies are attributable to hydroxides (532.0 eV) and chemisorbed H_2O (533.2 eV). Physisorbed –OH (excluding organic OH contaminants) content was calculated to be 3.9 %, 2.8 %, 0.9 %, and 2.4 % for mechanically polished (Fig. 5a), acid etched (Fig. 5b), chemically activated (Fig. 5c), and electrochemically activated (Fig. 5d) samples, respectively. This suggests that as the titanium alloy went through the steps of the activation processes, the physisorbed –OH decreased on the metal surface, while oxide layer thickened predominantly with the lattice oxide. In addition, it appears that chemical activation removed the physisorbed –OH from the surface more than the electrochemical activation.

During the electrochemical activation process in the alkaline solution, the naturally formed thin

titanium oxide is easily dissolved due to the reaction with OH^- to form $HTiO_3^-$. The subsequently exposed Ti is electrochemically oxidized in the alkaline solution possibly according to the following reaction (1):

$$Ti(s) + 3OH^-(aq.) - 3e \rightarrow TiO_2.H_2O + \frac{1}{2}H_2(g) \quad (1)$$

Gas evolution was observed on the Ti6Al4V substrate, possibly the result of hydrogen formation during the activation process. The XPS analysis shows that the O is mainly in the form of lattice oxide (O^{2-}) with small amount of hydroxide (physisorbed OH^-) and water (chemisorbed H_2O), thus the surface of activated substrate is dominated by hydrated TiO_2 and possibly Ti-OH^- hydrogel layer. The nanometer-scale pores formed during activation process may also demonstrate a capillary effect, which absorbs and retains the NaOH solution in the pores, resulting in a higher local pH on the surface. In addition to the bioactive TiO_2, the alkaline environment on the surface from both the capillary effect and Ti-OH^- layer is beneficial for the heterogeneous nucleation of hydroxyapatite on the surface, according to the following reaction (2):

$$10Ca^{2+}(aq.) + 6PO_4^{3-}(aq.) + 2OH^-(aq.) \leftrightarrow Ca_{10}(PO_4)_6(OH)_2 \quad (2)$$

This assumption was verified by surface pH measurement using pH indicators, shown in Table 2. These measurements revealed that the surface pH for untreated Ti6Al4V alloy was in the range of 5.2 to 7.4; and that for the chemically and electrochemically treated Ti6Al4V alloys were equal or greater than 8.2, which is favorable for the formation of hydroxyapaptite.

One of the main characteristics of metal oxides in aqueous solution is their point of zero charge (PZC), which represents the pH value of aqueous solution at which an immersed oxide surface has zero net charge. If the solution pH is greater than the pH at PZC of the metal oxide, the metal oxide is negatively charged; on the other side, if the solution pH is lower than the pH at PZC of metal oxide, the metal oxide is positively charged. The charged surface and surrounding solution forms a thin double layer, to which oppositely charged ions are attracted and initial reaction started between the charged metal oxide and the attracted ions. The PZC of the TiO_2 was reported to be in the range of 5.5 to 6.0 [31], resulting in a negatively charged surface in the coating solution at a pH of 6.50 in this investigation. Thus the positively charged Ca^{2+} is attracted to the surface of Ti6Al4V alloy and reacts with the TiO_2 to form $CaTiO_3$. The PZC of $CaTiO_3$ was reported as 8.1 [32], thus the $CaTiO_3$–covered surface is positively charged and the PO_4^{3-} is attracted to the surface to participate in further reactions, leading to the formation of calcium phosphate.

With the formation of calcium phosphate apatite on the surface, the super-saturation of simulated physiological solution may promote preferential nucleation of apatite on the already-formed apatite than in the solution due to the higher activation energy for the homogeneous nucleation of apatite in human body fluid. Thus the further formation of the apatite coating continues only on the initial apatite layer on the substrate by spontaneous growth consuming calcium and phosphate ions from the surrounding simulated body fluid. A theoretical analysis [33] also indicated that formation of hydroxyapatite exhibits a higher thermodynamic preference than that

of octacalcium phosphate (OCP) and dicalcium phosphate (DCP), thus the further formation of the coating proceeds in the form of hydroxyapatite, rather than OCP or DCP.

Due to the favorable surface condition and thermodynamics and kinetics of the hydroxapatite formation, hydroxyapatite coating can be deposited on the surface within a very short period of time at a practical deposition rate. The formed coating is shown in Fig. 6. Apatite coating initially deposits on the activated surface through heterogeneous nucleation, no precipitation is observed in the solution. Apatite may initially nucleate on activated sites, resulting in ball-like growth with un-even surface during the first 30 minutes of deposition following the contours of the surface ridges and valleys (Fig. 6a). The coating is of porous bone-like structure, and the whole substrate surface is fully covered with apatite coating within a short period of deposition. With the growth of hydroxyapatite, the coating grows thicker and eventually covers the valleys to form an even surface (Fig. 6b). The formed hydroxyapatite coating presents a similar surface morphology as the activated substrate, indicating a continuous deposition and growth of hydroxyapatite coating on the contours of the porous bone-like structure (Fig. 1).

The formed coating was scratched off the substrate and subjected to XRD analysis, and compared with the commercially available hydroxyapatite powders. The XRD spectrum is shown in Fig. 7. The XRD patterns (lower) of a commercial crystallized hydroxyapatite powder (PENTAX Corporation, Tokyo, Japan) match very well with the standard XRD pattern for HA in the JCPDF card. The major patterns (upper) of the coating powders are shown to match very well with the commercial HA powders, but with broader peaks possibly due to the nanocrystalline nature of the coating.

The sequential reactions involving Ca^{2+} and PO_4^{3-}, as well as the resulted hydroxyapatite coating were confirmed using EDX point analysis, which was conducted on the cross-section of a coated Ti6Al4V alloy sample (shown in Fig. 8).

The results of EDX point analysis on the hydroxyapatite coating and corresponding ratios of Ca/P are listed in Table 3. Measurements 3 and 4 close to the substrate show the coexistence of Ca, Ti, V or P, indicating a preferential formation of Ca on the Ti6Al4V surface at the initial stage of deposition (There is no phosphorus detected in measurement 3). The phosphorus then participates for subsequent deposition, as is evident in measurement 4 that is away from the substrate surface. This effect is further evident by the eventual formation of hydroxyapatite shown by measurements 1, 2 and 5. The ratio of Ca/P in the initial layer (measurement 3 and 4) is deviated far from stoichometric hydroxyapatite. Measurements 1, 2 and 5 are away from the initial deposition layer and the substrate, the average of Ca/P ratio of these three measurements is 1.67, which is exactly the atomic ratio of Ca/P in stoichometric hydroxyapatite ($Ca_{10}(PO_4)_6(OH)_2$).

Imaging analysis using SEM micrograph was conducted to measure pore size of the hydroxyapatite coating. The mean values of two measurements are shown in Table 4. The measurements show that most of the pores are in the range of 160 – 800 nm.

TEM analysis (Fig. 9) shows that the nanometer-scale hydroxyapatite crystals were deposited on the surface of the activated titanium alloy with a grain size of less than 20nm (Fig. 9a). The

micrograph of one single hydroxyapatite plate (Fig. 9b) also demonstrates that the grain of the formed hydroxyapatite is less than 20 nm in size. The formed nanocrystalline hydroxyapatite mimics the composition and crystal structure of natural bone. The grain refinement to nanometer scale enhances bioactivity and biocompatibility, and increases the strength of the formed hydroxyapatite coating and reduces the wear of the materials.

4. Conclusions

Electrochemical activation is an effective and economic method to modify the surface topography and chemistry to promote the formation of biocompatible hydroxyapatite layer on Ti6Al4V alloy by creating nanometer-scale pores aligning perpendicularly to the surface and elevating the surface pH. The initial layer may be formed with a sequential participation of Ca^{2+} and PO_4^{3-}. The continuation of deposition proceeds to form pure hydroxyapatite, confirmed by XRD and EDX point analysis. The formed hydroxyapatite coating is confirmed of nanometer-scale grain size from TEM analysis.

Acknowledgements

This project is financially supported by CIHR-NRC Science and Technology Convergence Program for Innovation. The authors are grateful to Mr. R. Davidson in University of Western

Ontario for the FESEM observation and XPS analysis, Mr. J. Nagata in IMTI for technical support.

References

1. Lausmaa J, Kasemo B and Mattsson H. Surface spectroscopic characterization of Titanium implant materials. Appl Surf Sci 1990; 44: 133-146.
2. McCafferty E and Wightman JP. An X-ray photoelectron spectroscopy sputter profile study of the native air-formed oxide film on titanium. Appl Surf Sci 1999; 143: 92-100.
3. Pouilleau J, Devilliers D, Garrido F, Durand-Vidal S and Mahé E. Structure and and composition of passive titanium oxide films. Mat Sci Eng 1997; B47:235-243.
4. Williams DF. Titanium for medical applications. In: Brunette DM, Tengvall P, Textor M. and Thomsen P, editors. Titanium in medicine: materials science, surface science, engineering, biological responses and medical applications. New York: Springer-Verlag Berlin Heidelberg; 2001. p 13-24.
5. Kim HM, Miyaji F, Kokubo T and Nakamura T. Preparation of bioactive Ti and its alloys via simple chemical surface treatment. J Biomed Mater Res 1996; 32: 409-417.
6. Kokubo T. Apatite formation on surfaces of ceramics, metals and polymers in body environment. Acta Mater 1998; 46: 2519-2527.
7. Yao C, Slamovich EB, Webster TJ. Titanium nanosurface modification by anodization for orthopedic application. Mater Res Soc Symp Proc 2005; 845: 215-220.

8. Hata K and Kokubo T. Growth of a bonelike apatite layer on a substrate by biomimetic process. J Am Ceram Soc 1995; 78: 1049-1053.
9. Tang Y, Liu Y, Sampathkumaran U, Hu MZ, Wang R and de Guire MR. Particle growth and particle surface interaction of ceramic thin films. Solid State Ionics 2002; 151: 69-78.
10. Barrere F, Layrolle P, van Bliterswijk CA and de Groot K. Biomimetic calcium phosphate coatings on Ti6Al4V: A crystal growth study of octacalcium phosphate and inhibition by Mg^{2+} and HCO_3^-. Bone 1999; 25: 107S-111S.
11. Kasuga T, Kondo T and Nogami M. Apatite formation on TiO_2 in Simulated body fluid. J Cryst Growth 2002; 235: 235-240.
12. Hayakawa S and Osaka A. Biomimetic deposition of calcium phosphates on oxides soaked in a simulated body fluid. J Non-Cryst Solids 2000; 263&264: 409-415.
13. Gil FJ, Padros A, Manero JM, Aparicio C, Nilsson M and Planell JA. Growth of bioactive surfaces on titanium and its alloys for orthopaedic and dental implants. Mater Sci Eng C 2002; 22: 53-60.
14. Zhang JM, Lin CJ, Feng ZD and Tian ZW. Mechanistic studies of electrodeposition for bioceramic coatings of calcium phosphate by an in situ pH-microsensor technique. J Electroanal Chem 1998; 452: 235-240.
15. Okido M, Kuroda K, Ishikawa M, Ichino R and Takai O. Hydroxyapatite coating on titanium by means of thermal substrate method in aqueous solutions. Solid State Ionics 2002; 151: 47-52.
16. Wang J, Layrolle P, Stigter M and de Groot K. Biomimetic and electrolytic calcium phosphate coatings on titanium alloy: physicochemical characteristics and cell attachment. Biomaterials 2004; 25: 583-592.

17. Jonášová L, Müller FA, Helebrant A, Strnad J and Greil P. Biomimetic apatite formation on chemically treated titanium. Biomaterials 2004; 25: 1187-1194.

18. Monma H. Electrolytic deposition of calcium phosphates on substrate. J Mater Sci 1994; 29: 949-953.

19. Chen JS, Juang HY, Hon MH. Calcium phosphate coating on titanium substrate by a modified electrocrystallization process. J Maters Sci: Mater M 1998; 9: 297-300.

20. Stoch A, Brożek A, Kmita G, Stoch J, Jastrzębski W and Rakowska A. Electrophoretic coating of hydroxyapatite on titanium implants. J Mol Struct 2001; 596: 191-200.

21. Kim KM, Koh YH, Li LH, Lee S and Kim HE. Hydroxyapatite coating on titanium substrate with titania buffer layer processed by sol-gel method. Biomaterials 2004; 25: 2533-2538.

22. Shirkhanzadeh M. Calcium phosphate coatings prepared by electrocrystallization from aqueous electrolytes. J Mater Sci: Mater M 1995; 6: 90-93.

23. Barrere F, Snel MME, van Blitterswijk CA, de Groot K and Layrolle P. Nanometer-scale study of the nucleation and growth of calcium phosphate coating on titanium implants. Biomaterials 2004; 25: 2901-2910.

24. Wen HB, de Wijn JR, Cui FZ and de Groot K. Preparation of bioactive Ti6Al4V surfaces by a simple method. Biomaterials 1998; 19: 215-221.

25. Feng QL, Wang H, Cui FZ and Kim TN. Controlled crystal growth of calcium phosphate on titanium surface by NaOH-treatment. J Cryst Growth 1999; 200: 550-557.

26. Wen HB, Wolke JGG, de Wijn JR, Liu Q, Cui FZ and de Groot K. Fast precipitation of calcium phosphate layers on titanium induced by chemical treatments. Biomaterials 1997; 18: 1471-1478.

27. Liang F, Zhou L and Wang K. Apatite formation on porous titanium by alkali and heat-treatment. Surf Coat Tech 2003; 165: 133-139.

28. Li F, Feng QL, Cui FZ, Li HD, and Schubert H. A simple biomimetic method for calcium phosphate coating. Surf Coat Tech 2002; 154: 88-93.

29. Feng QL, Cui FZ, Wang H, Kim TN and Kim JO. Influence of solution conditions on deposition of calcium phosphate on titanium by NaOH-treatment. J Cryst Growth 2000; 210: 735-740.

30. Kim HM, Miyazaki T, Kokubo T and Nakamura T. Revised simulated body fluid. Key Eng Mater 2001; 192-195: 47-50.

31. Kosmulski M. The pH-dependant surface charging and the points of zero charge. J Colloid Interf Sci 2002; Vol. 253: 77-87.

32. Hanawa T, Kon M, Doi H, Ukai H, Murakami K, Hamanaka H and Asaoka K. Amount of hydroxyal radical on calcium-ion-implanted titanium and point of zero charge of constituent oxide of the surface-modified layer. J Mater Sci: Mater M 1998; 9: 89-92.

33. Lu X, Leng Y. Theoretical analysis of calcium phosphate precipitation in the simulated body fluid. Biomaterials 2005; 26: 1097-1108.

List of Figures

Fig. 8 EDX point analysis on the cross-section of apatite-coated Ti6Al4V alloy

Fig. 9 TEM analysis of (a) the nano-sized grains and crystal planes, (b) the morphologies of the nano-sized hydroxyapatite grains

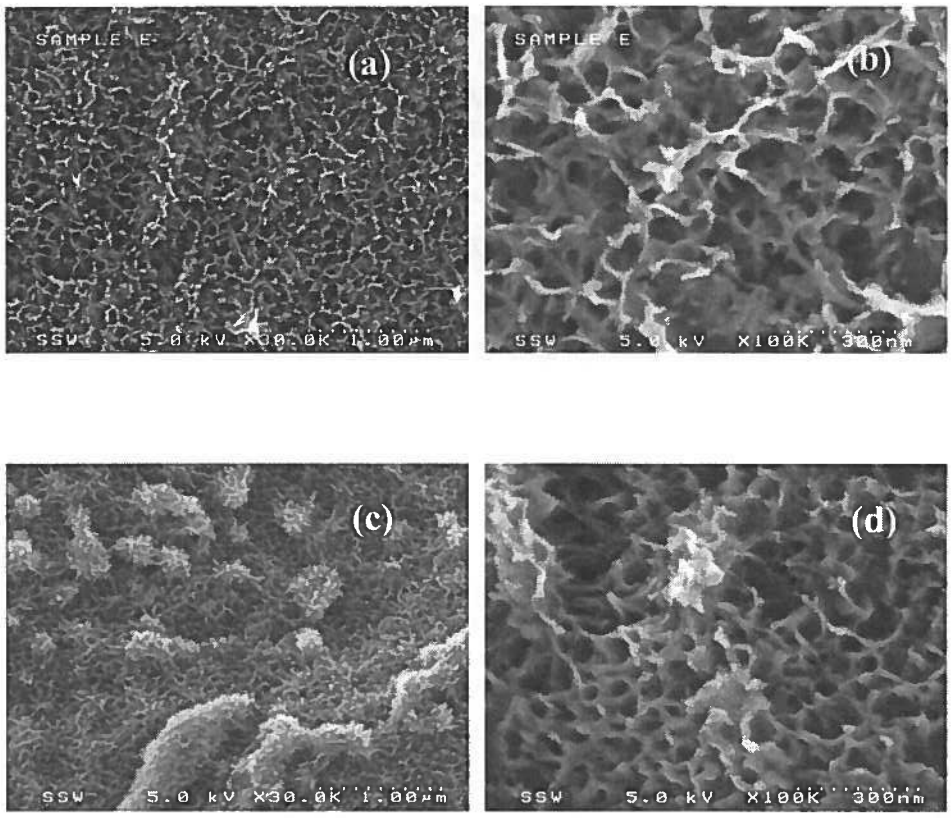
SAMPLE E
(a)
SSW 5.0 kV X30.0K 1.00µm
SAMPLE E
(b)
SSW 5.0 kV X100K 300nm
(c)
SSW 5.0 kV X30.0K 1.00µm
(d)
SSW 5.0 kV X100K 300nm

Fig. 1

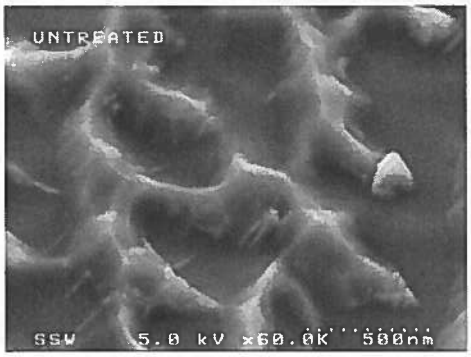

Fig. 2

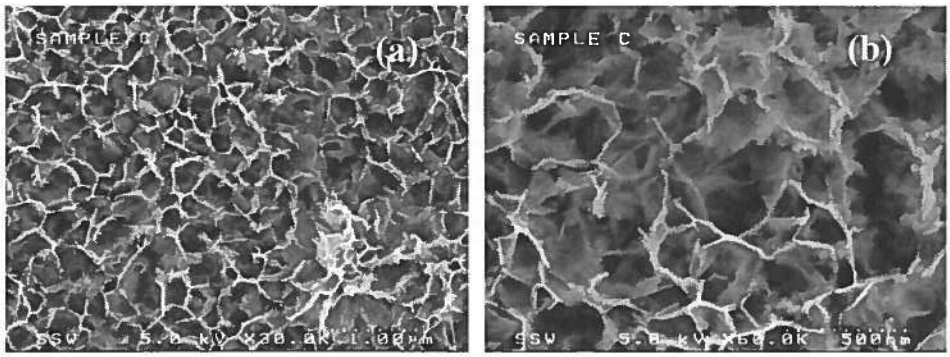

Fig. 3

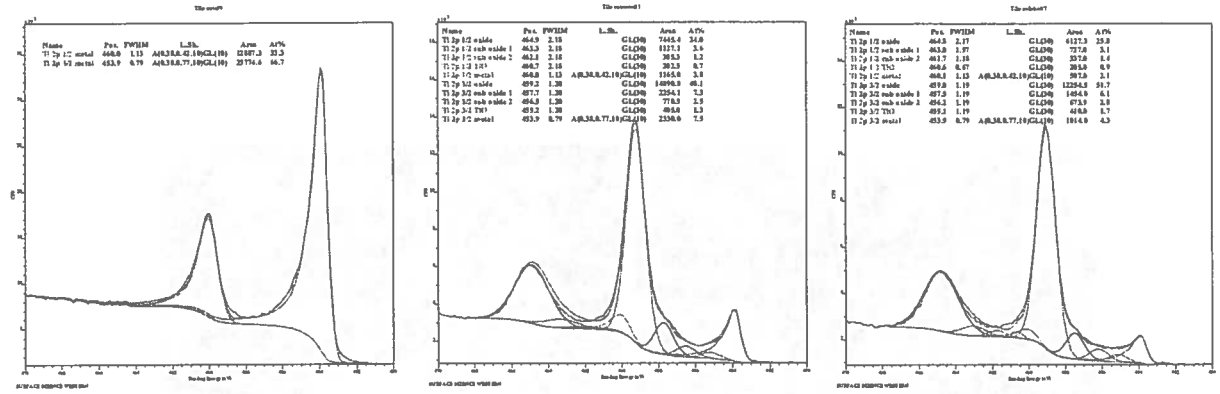

(a) (b) (c)

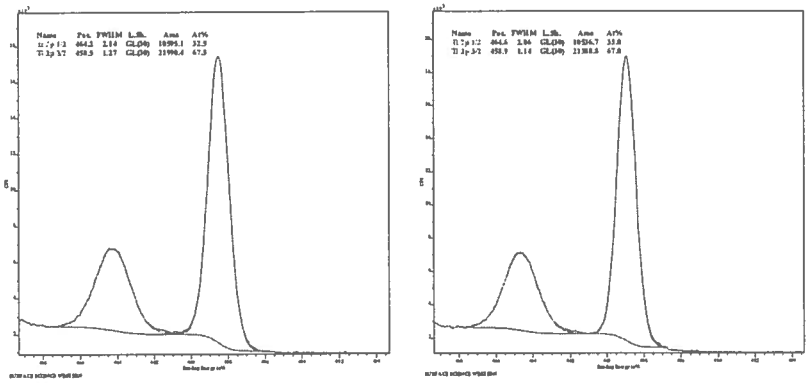

(d) (e)

Fig. 4

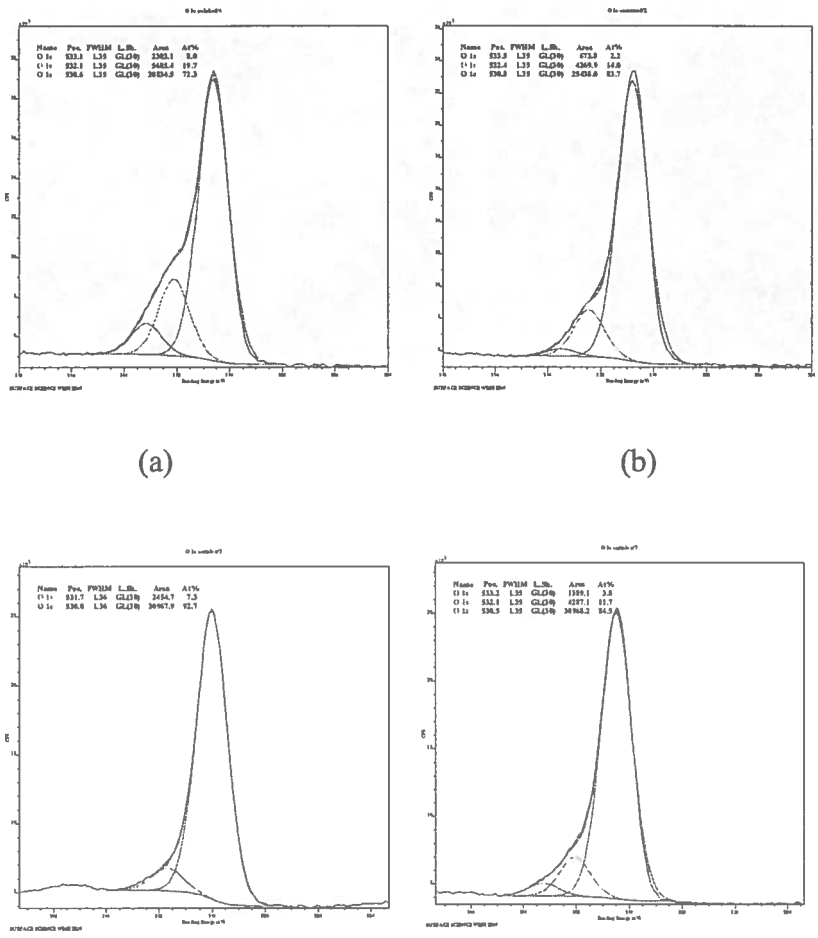

(a) (b)

(c) (d)

Fig. 5

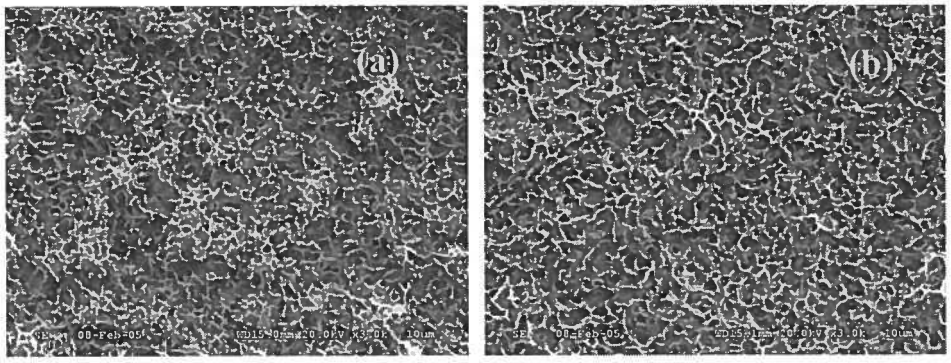

Fig. 6

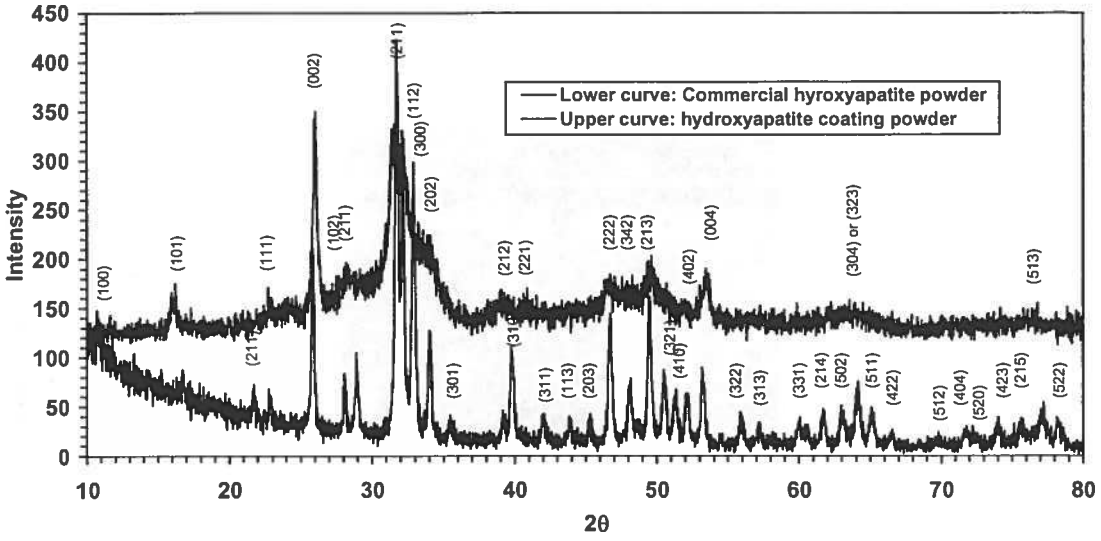
Lower curve: Commercial hyroxyapatite powder
Upper curve: hydroxyapatite coating powder
Intensity
2θ
(100)
(101)
(111)
(002)
(102)
(211)
(112)
(300)
(202)
(212)
(221)
(222)
(342)
(213)
(402)
(004)
(304) or (323)
(513)
(301)
(311)
(113)
(203)
(322)
(313)
(331)
(214)
(502)
(511)
(422)
(512)
(404)
(520)
(423)
(215)
(522)

Fig. 7

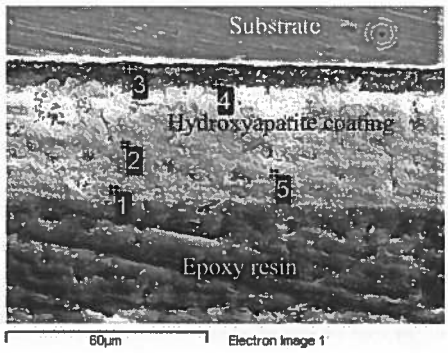
Substrate
3
4
Hydroxyapatite coating
2
5
1
Epoxy resin
60µm
Electron Image 1

Fig. 8

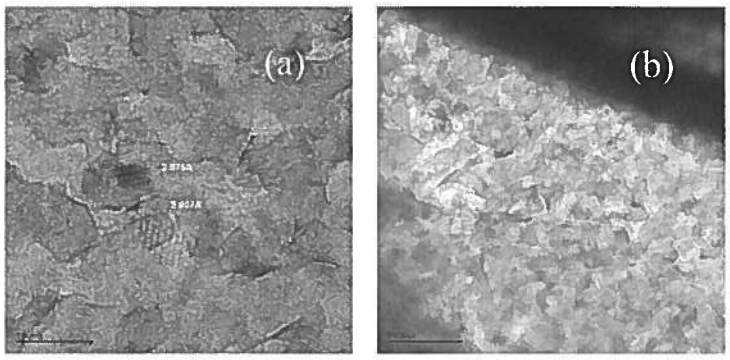

Fig. 9

Table 2

Indicators		Methyl orange	Bromocresol purple	m-Cresol purple	Phenolphthalein
Properties of indicators	pH range	3.2 – 4.4	5.2 – 6.8	1.2 – 2.8; 7.4 – 9.0	8.2 – 10.0
	Color change	Red to yellow	Yellow to purple	Red to yellow; yellow to purple	Color to pink
Reactions of samples to indicators	Untreated	To yellow	To purple	To yellow	No change
	Chemical treatment				To pink
	Constant Potential				To pink
	Constant Voltage				To pink

Table 3

	Measurement	C	O	P	Cl	Ca	Ti	V	Ca/P	Average
Initial Layer	3	21.80				21.47	51.55	5.19	**N/A**	**N/A**
	4	32.71	25.72	5.25		21.47	13.68	1.23	**4.08**	
Bulk Coating	2	58.04	18.72	8.33	0.56	14.35			**1.72**	**1.67**
	5	64.56	18.11	6.36	0.36	10.59			**1.67**	
	1	67.77	16.43	5.81	0.52	9.47			**1.63**	

Table 4

Measurement 1	Mean diameter (μm)	0.201	0.511	0.831	1.148	1.495	1.785	2.094	2.722
	Mean length (μm)	0.162	0.599	1.181	1.790	2.456	2.911	3.686	5.890
	Percentage (%)	55.98	33.59	7.14	2.14	0.67	0.31	0.09	0.04
Measurement 2	Mean diameter (μm)	0.314	0.647	0.968	1.321	1.620	1.907	2.106	3.007
	Mean length (μm)	0.300	0.848	1.483	2.134	2.813	3.412	3.717	6.039
	Percentage (%)	64.05	17.13	4.06	1.16	0.58	0.09	0.04	0.09